Journal of Medicinal Chemistry

Article

pubs.acs.org/jmc

# Optimization of Inhibitors of the Tyrosine Kinase EphB4. 2. Cellular Potency Improvement and Binding Mode Validation by X-ray Crystallography

Karine Lafleur,[†,‡,#] Jing Dong,[‡,#] Danzhi Huang,[‡] Amedeo Caflisch,[*,‡] and Cristina Nevado[*,†]

[†]Department of Organic Chemistry and [‡]Department of Biochemistry, University of Zurich, Winterthurerstrasse 190, CH-8057 Zurich, Switzerland

Supporting Information

**ABSTRACT:** Inhibition of the tyrosine kinase erythropoietin-producing human hepatocellular carcinoma receptor B4 (EphB4) is an effective strategy for the treatment of solid tumors. We have previously reported a low nanomolar ATP-competitive inhibitor of EphB4 discovered in silico by fragment-based high-throughput docking combined with explicit solvent molecular dynamics simulations. Here we present a second generation of EphB4 inhibitors that show high inhibitory potency in both enzymatic and cell-based assays while preserving the appealing selectivity profile exhibited by the parent compound. In addition, respectable levels of antiproliferative activity for these compounds have been obtained. Finally, the binding mode predicted by docking and molecular dynamics simulations is validated by solving the crystal structures of three members of this chemical class in complex with the EphA3 tyrosine kinase whose ATP-binding site is essentially identical to that of EphB4.

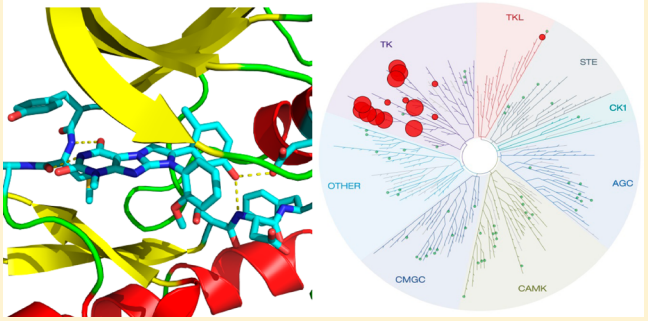


## INTRODUCTION

Protein kinases are involved in the phosphorylation of signaling proteins and regulate key processes such as cell differentiation, cell proliferation, and cell motility. Depending on their target residue, protein kinases can be divided into serine-threonine and tyrosine kinases. Receptor tyrosine kinases (RTKs) are transmembrane proteins which, upon interactions with their cognate ligands, undergo dimerization and autophosphorylation. Subsequent phosphorylation of cytoplasmic proteins by the activated receptor triggers a signaling cascade which, in turns, induces the transcription of specific genes. Thus, disruption of the protein function or aberrant protein expression has been linked to several types of diseases, including cancer.

Eph (erythropoietin-producing human hepatocellular carcinoma) kinases represent the largest family of RTKs. They are divided into two families, EphA and EphB, which interact with ephrinA and ephrinB ligands, respectively.[1] Interactions between Eph receptors and ephrin ligands induce a forward signaling and a ligand reverse signaling involved in cell adhesion, repulsion, and migration. Depending on the type of tumor, Eph−ephrin interactions have been shown to either promote or inhibit tumor growth. Interestingly, several studies have implicated EphB4−ephrinB2 signaling in sprouting angiogenesis and blood vessel maturation,[2] and the inhibition of vascular endothelial growth factor (VEGFR)-driven angiogenesis by a selective EphB4 inhibitor has recently been described.[3] Therefore, inhibition of EphB4 activity has been recognized as an effective strategy for the therapy of solid tumors. ATP-competitive EphB4 inhibitors of type I,[4,5] type $I_{1/2}$,[6,7] and type II[3,8] have been discovered and recently reviewed.[9]

We have previously reported the identification of two series of low micromolar ($\mu$M) type I inhibitors of EphB4 by fragment-based high-throughput docking.[10] Starting from a library of about 700 000 compounds, our computational strategy was designed to generate a focused subset of molecules with promising anchor fragments for the ATP binding site of EphB4. Automatic docking of the 21 418 compounds of the focused library and subsequent in vitro evaluations yielded compounds **1** and **2**, which inhibit EphB4 enzymatic activity in the low micromolar range (Table 1).[10] Their predicted binding mode involves two hydrogen bonds between the pyrimidine ring and the Met696 backbone polar groups in the so-called hinge region of the ATP binding pocket (Figure 1, left). Guided by the binding mode predicted by docking and further validated by explicit solvent molecular dynamics simulations, a tailored library of derivatives of the parent scaffold was synthesized to improve the binding affinity.[6] In fact, addition of a methyl and a hydroxyl group at positions 2 and 5 of the phenyl ring, respectively, provided compound **3** (Figure 1, right), which shows single-digit nanomolar potency in two different enzymatic assays with the kinase domain of EphB4 in

**Received:** August 12, 2012
**Published:** December 19, 2012

**Table 1. EphB4 Inhibition Data of Xanthine Derivatives**

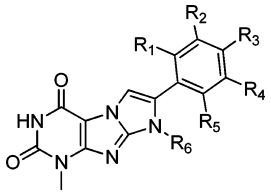


| | | | | | | | enzymatic assay $IC_{50}$ (nM) | | |
|---|---|---|---|---|---|---|---|---|---|
| compound | $R_1$ | $R_2$ | $R_3$ | $R_4$ | $R_5$ | $R_6$ | FRET[a] | radiometric[b] | cellular assay $IC_{50}$ (nM)[c] |
| **1** | H | H | H | H | H | *o*-methoxyphenyl | 3300 | 4350 | 14% at 20 $\mu$M |
| **2** | H | H | H | H | H | butyl | 1900 | 538 | <10% at 20 $\mu$M |
| **3** | Me | H | H | OH | H | *o*-methoxyphenyl | 5 | 1.6 | 130 |

[a]FRET-based enzymatic assay carried out using the Z′-LYTE Kinase Assay Kit−Tyr 1 Peptide (Invitrogen, Grand Island, NY) following the vendor instructions. [b]Measured at Reaction Biology Corporation using radiolabeled ATP. [c]Cell $IC_{50}$ values for compounds **1** and **2** were measured in a cellular phosphorylation assay using CHO cells overexpressing EphB4. For compound **3**, measurements were performed at Proqinase using MEF cells overexpressing EphB4.

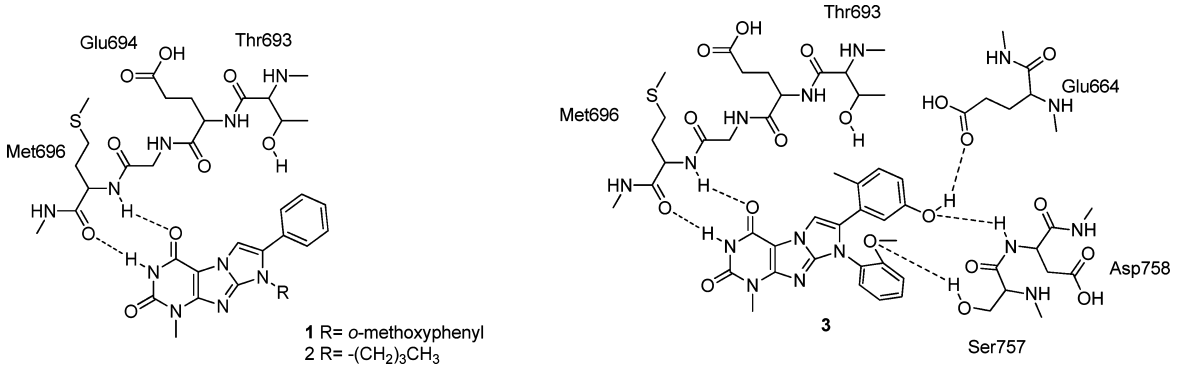


**Figure 1.** (Left) Predicted binding mode of compounds **1** and **2**.[10] (Right) Binding mode of compound **3** as predicted in silico and validated by X-ray crystallography. The EphB4 residues involved in binding are shown. Thr693 is the so-called gatekeeper residue while Asp758 is the first residue in the DFG motif.

solution (Table 1). In addition, compound **3** showed a promising selectivity profile (Figure 2, right). Unfortunately, a significant reduction of inhibitory activity on EphB4 was observed for this compound in a cellular assay compared to the enzymatic assays. This discrepancy could be due to reduced permeability or increased efflux of the molecule by active transporters. In addition, phenols can undergo glucuronidation during phase II metabolism, thus having poor pharmacokinetic properties.[11,12]

With these results in hand, we embarked on a multidisciplinary optimization campaign aimed at the development of a second generation of EphB4 inhibitors that combine high inhibitory potency in both enzymatic and cell-based assays while retaining the appealing selectivity profile exhibited by the parent compound. Here, we present the validation of this approach, which has led to the discovery of a lead compound incorporating not only high potency and selectivity but also a promising pharmacological profile as well as respectable levels of antiproliferative activity. In addition, we report herein the confirmation of the binding mode of this chemical class to the Eph receptor tyrosine kinase by means of X-ray crystallography.

## ■ LEAD OPTIMIZATION STRATEGY

In line with the results obtained in the enzymatic assay, the inhibition activity of compounds **1** and **2** on EphB4-transfected Chinese hamster ovary (CHO) cells has been shown to be relatively low with $IC_{50}$ values in the high micromolar range.[10]

The high potency displayed by compound **3** in the enzymatic assay prompted us to explore its activity on a cellular setting. Thus, cellular phosphorylation assays were carried out on murine embryonal fibroblast cells (MEF) transfected with myc-tagged human EphB4 (Proqinase). After incubation with the corresponding inhibitor and stimulation with ephrinB2-Fc, autophosphorylation of EphB4 was quantified via sandwich ELISA. While compound **3** showed single-digit nanomolar activity in enzymatic assay, its inhibition activity in cells was reduced by almost 2 orders of magnitude, with $IC_{50}$ values higher than 100 nM (Table 1). There are multiple reasons for a discrepancy between enzymatic and cellular assays, including the passage through the cell membrane, the natural environment, and relevant ATP concentration present only in the latter.[13] To further evaluate the pharmacological potential of compound **3**, its cell permeability was investigated first. While passive transport was assessed on Caco-2 monolayers, active efflux was tested on P-glycoprotein and BCRP transporters (Absorption Systems). Caco-2 cells express many transport proteins present on epithelial cells of the small intestine and form tight junctions between each other. Thus, measurements of permeability through Caco-2 monolayers may also predict absorption across intestinal tissues in vivo. Interestingly, compounds **1** and **2** bearing hydrogens at position $R_1$ and $R_4$ showed high cell permeability, the latter showing the highest membrane permeation, while no significant efflux was observed (Table 2). In contrast, compound **3** with a methyl group at $R_1$


dx.doi.org/10.1021/jm301187e | J. Med. Chem. 2013, 56, 84−96

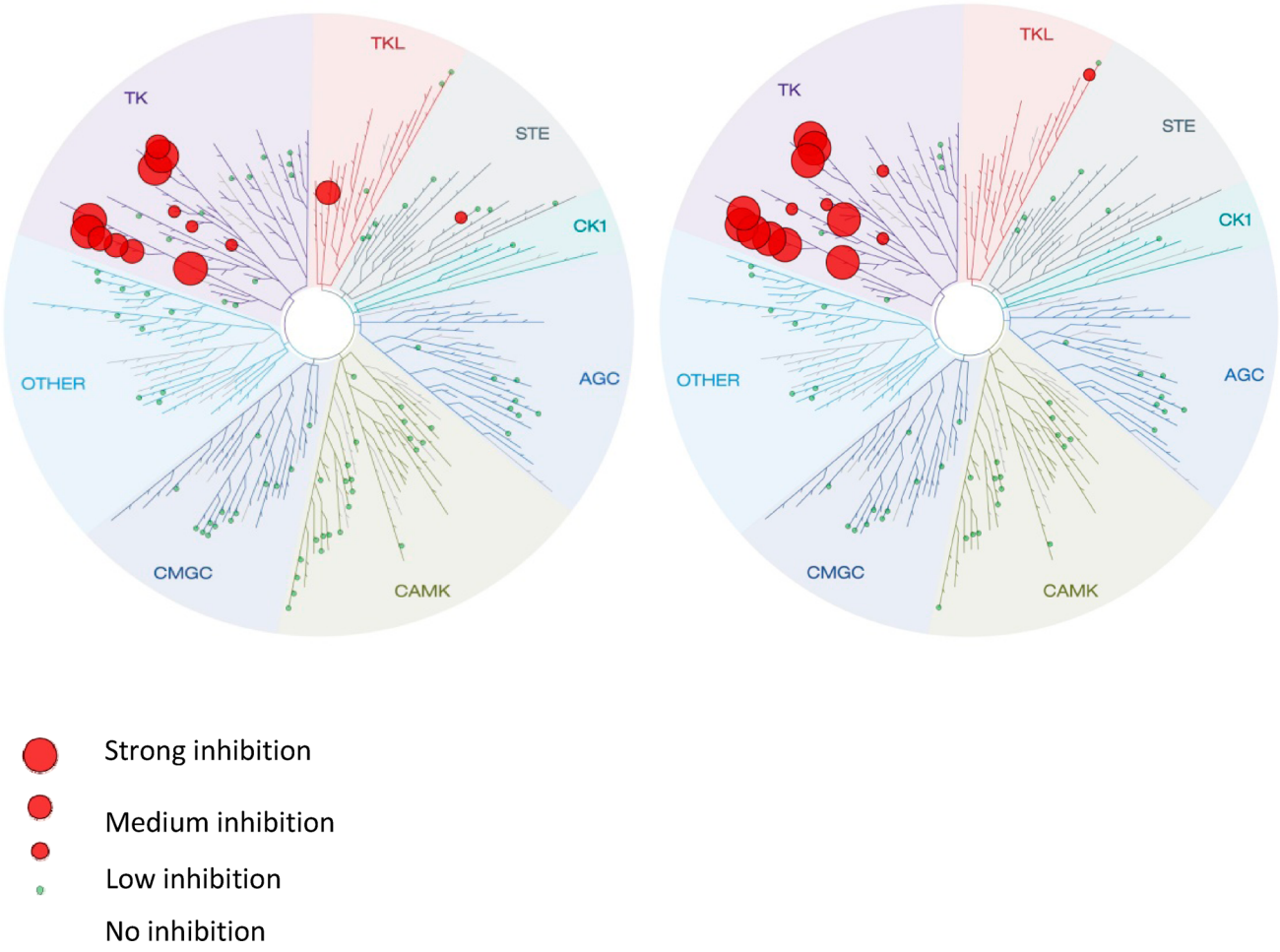


**Figure 2.** Selectivity profile of compound **40** (left) and **3** (right) tested on a panel of 124 protein kinases. Measurements were performed at the University of Dundee using a [$\gamma$-$^{33}$P]ATP-based enzymatic assay at a concentration of 3 $\mu$M for compound **40** and 1 $\mu$M for compound **3**. The affinity is defined as strong, medium, and low (corresponding to <10%, 10−30%, and 30−70%, respectively, of remaining activity with respect to a DMSO control). The dendrogram was obtained from KinomeScan using the KinomeTree software.

**Table 2. Cell Permeability Measurements for Compounds 1−3 Using the Caco-2 Model**

| | % recovery | | $P_{app}$ ($\times 10^{-6}$ cm/s)[a] | | | | |
|---|---|---|---|---|---|---|---|
| compound | A−B | B−A | A−B | B−A | efflux ratio[b] | permeability classification[c] | significant efflux[d] |
| **1** | 71 | 76 | 32.3 | 35.8 | 1.1 | high | no |
| **2** | 69 | 78 | 42.5 | 42.5 | 1.0 | high | no |
| **3** | 51 | 74 | 3.13 | 23.0 | 7.3 | high | yes |

[a]Apparent permeability ($P_{app}$) is measured from the apical side to the basolateral side (A−B) and from the basolateral side to the apical side (B−A). [b]Efflux ratio = ($P_{app}$ B → A)/($P_{app}$ A → B). [c]Permeability classification: low = ($P_{app}$ A → B) < $1.0 \times 10^{-6}$cm/s; high = ($P_{app}$ A → B) > $1.0 \times 10^{-6}$ cm/s. [d]Significant efflux: efflux ratio > 3.0 and ($P_{app}$ B → A) > $1.0 \times 10^{-6}$ cm/s.

and a hydroxyl group at $R_4$ showed high cell permeability although it was significantly effluxed by P-glycoprotein transporters, which could explain the activity discrepancy between enzymatic and cellular assays.

As phenols are known to be detrimental for the pharmacokinetic properties of drugs,[11,12] we decided to remove the hydroxyl group at position $R_4$. In addition, replacement of the anisidine side chain by an alkyl chain appeared to be promising, according to the permeability measurements (compare compounds **1** with $P_{app}$ = $32.3 \times 10^{-6}$ cm/s and **2** with $P_{app}$ = $42.5 \times 10^{-6}$ cm/s in Table 2). Thus, we investigated the synthesis of molecules bearing a methyl group at position $R_1$ and a butyl, pentyl, or hexyl chain at position $R_6$ (a previous shortening of the alkyl chain did not improve the affinity to EphB4; see ref 10). In addition, we also decided to introduce a fluorine at position $R_3$, To explore the possibility of the potential formation of an additional halogen bond between the inhibitor and the Glu664 residue,[14,15] we also examined the addition of a chlorine at position $R_4$. To improve the van der Waals interactions between the ligand and the side chains of Val629, Ala645, and Thr693, we also aimed at introducing a chlorine atom or a trifluoromethyl group at position $R_1$, with $R_6$ being either an alkyl chain or an aromatic ring.

Rigidification of biologically active molecules has been shown to be beneficial for selectivity properties,[11] as the number of accessible conformations able to interact with secondary targets


dx.doi.org/10.1021/jm301187e | J. Med. Chem. 2013, 56, 84−96

**Scheme 1**[a]

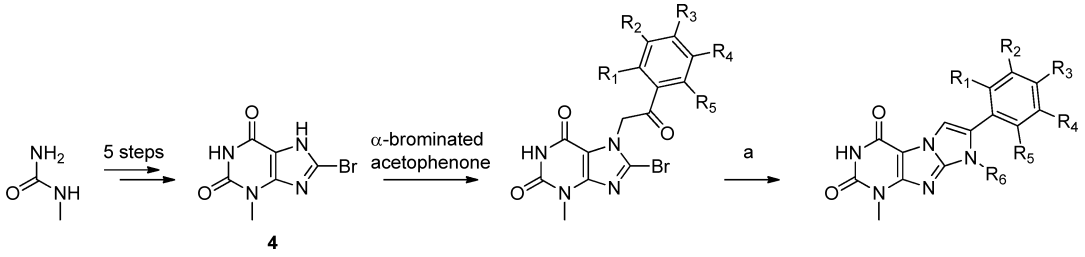


[a]Reagents and conditions: (a) Primary amine, EtOH, reflux, 15 h.

**Scheme 2**[a]

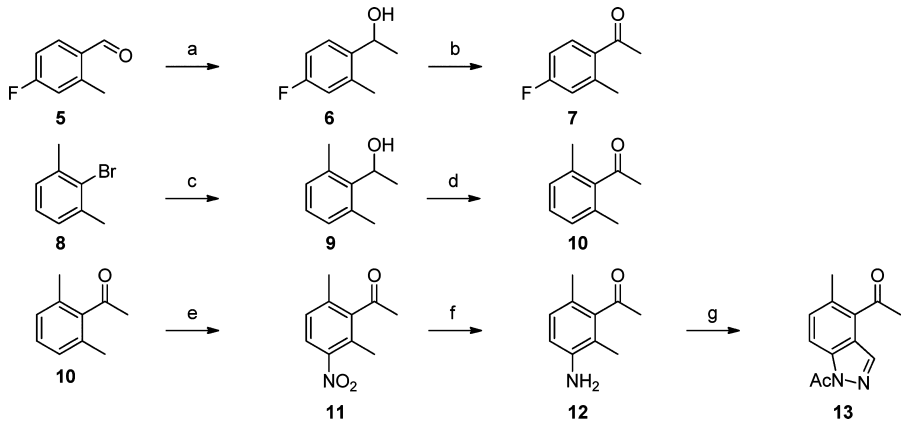


[a]Reagents and conditions: (a) MeLi, THF, 25 °C, 1 h, 55%. (b) PCC, $CH_2Cl_2$, 25 °C, 1 h, 73%. (c) BuLi, acetaldehyde, THF, −78 °C, 1.5 h. (d) PCC, $CH_2Cl_2$, 25 °C, 1 h, 56% yield over two steps. (e) $KNO_3$, $H_2SO_4$, 0 °C, 1 h. (f) Fe, AcOH, EtOH, 90 °C, 2 h, 47% yield over two steps. (g) NaOAc, $Ac_2O$, $CHCl_3$, 25 °C, 30 min, then iAmONO, 60 °C, 7 h, 58%.

is restricted. In addition, ortho-substitution of bicyclic molecules with methyl or methoxy groups has been shown to decrease crystal packing and improve aqueous solubility.[16] We therefore investigated the synthesis of a bis-*ortho*-methyl-substituted phenyl ring on the xanthine scaffold. Finally, poor oral bioavailability of kinase inhibitors entitling an *ortho*-methyl/*meta*-hydroxyphenyl pattern[11,17,18] led to the replacement of the phenol ring by an indazole moiety.[11] This transformation aimed to generate a molecule with a similar hydrogen bonding pattern as compound **3** with EphB4.

With these designs in mind, we set out to explore the synthesis of a small set of customized analogues to later evaluate their biochemical and pharmacological profile.

## SYNTHESIS

Recently, a growing interest in the synthesis of imidazoxanthines has emerged, as a few derivatives proved to be potent serotonin,[19] $A_3$ adenosine,[20,21] or kinase receptor antagonists.[6] Following our previously developed route, the synthesis of the key intermediate 3-methyl-8-bromoxanthine **4** was achieved in five steps starting from the corresponding alkylurea (Scheme 1). After alkylation with α-brominated acetophenones, cyclization usually occurs by refluxing the resulting intermediate in ethanol in the presence of a primary amine.[6,19,20] However, to the best of our knowledge, the synthesis of bis-ortho-substituted imidazoxanthines has not been described yet. In addition, none of the mono-ortho-substituted molecules reported so far has an alkyl chain at position $R_6$.

The synthesis of the noncommercially available acetophenones used in the preparation of this new set of inhibitors is summarized in Scheme 2. Treatment of commercially available 4-fluoro-2-methylbenzaldehyde **5** with methyllithium followed by oxidation with PCC provided methyl ketone **7** in 40% yield over two steps. The synthesis of 1-(2,6-dimethylphenyl)-ethanone started with 2-bromo-1,3-dimethylbenzene **8**, which undergoes bromo−lithium exchange in the presence of nBuli, followed by reaction with acetaldehyde to afford secondary alcohol **9**. Subsequent oxidation using PCC gave the expected acetophenone **10**,[22] which was used as starting material in the synthesis of 1,1′-(5-methyl-1*H*-indazole-1,4-diyl)diethanone **13**. Indeed, reaction with $KNO_3$ selectively nitrated compound **10** at the meta position relative to the carbonyl group.[23] Reduction in the presence of iron and cyclization using isoamyl nitrite afforded the protected indazole derivative **13** in good to moderate yields.[24]

α-Bromination of the acetophenones reported in Scheme 2 as well as the commercially available 2′-chloroacetophenone (**14**), 3′-chloroacetophenone (**15**), and 2′-(trifluoromethyl)-acetophenone (**16**), was achieved in the presence of copper(II) bromide in chloroform as shown in Scheme 3.[25]

Alkylation at the $N_7$ position of bromoxanthine **4** with meta-substituted or mono-ortho-substituted α-haloketones was accomplished using *N*,*N*-diisopropylethylamine in DMF to give intermediates **24**−**27** (Scheme 4). To our surprise, in contrast to our previous experience with anilines, the subsequent cyclization with alkylamines under the standard conditions shown in Scheme 1 was never observed. Instead, only intermediates **31**−**36** could be isolated from the reaction mixtures probably due to the more electron-rich nature of alkylamines, which are able to accomplish not only the


dx.doi.org/10.1021/jm301187e | J. Med. Chem. 2013, 56, 84−96

**Scheme 3**[a]

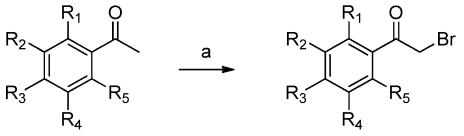


[a]Reagents and conditions: (a) $CuBr_2$, $CHCl_3$, EtOAc, reflux, 15 h (21–64% yield).

substitution of the bromine at $C_8$ but also the condensation with the carbonyl group. Fortunately, upon imine activation in the presence of a Lewis acid such as aluminum trichloride, the expected cyclization products **40**–**45** could be obtained in good yields. Interestingly, when position $R_1$ was substituted by a trifluoromethyl group, the reaction with butylamine gave the substitution product **37**, which could be then converted into **46** upon treatment with the amine in the presence of $AlCl_3$.

Cyclization of the derivatives bearing chlorine atoms at positions $R_1$ and $R_4$ in the presence of anisidine was performed as previously reported,[6] giving products **47** and **48** (Scheme 5).

The synthesis of derivatives bearing a bis-ortho-phenyl-substituted ring also proved to require further adjustments of the synthetic sequence as summarized in Scheme 6. The alkylation of **4** with bis-ortho-substituted $\alpha$-haloketones **18** and **19** required heating, but now the subsequent cyclizations in the presence of anisidine failed. The reactions with butylamine provided the substitution products **38** and **39**, which could finally be cyclized by heating in a concentrated solution of boron trifluoride diethyl etherate to give compounds **49** and **50**. Note that the reaction with butylamine also deprotected the acetylated intermediate **30**.

## ENZYMATIC, CELL-BASED ASSAY AND EVALUATION OF CELL PERMEABILITY

The inhibitory activity of our second generation of EphB4 inhibitors **40**–**50** was first evaluated on an enzymatic assay based on fluorescence resonance energy transfer (FRET). Additionally, compounds **40**, **43**, and **50** were also tested in a cell-free enzymatic assay based on radiolabeled ATP (Table 3). Removal of the hydroxyl group at $R_4$ and replacement of the anisidine by a butyl group yielded **40** with an $IC_{50}$ around 50 nM, thus reflecting the beneficial effect of an alkyl lateral chain (see also Table 1, entries 1 and 2). Elongation of the butyl chain (compounds **41** and **42**) did not improve the affinity, which is congruent with the orientation toward solvent of the alkyl chain. The introduction of a fluorine atom at position $R_3$ yielded compound **43** with binding affinity similar to that of compound **40** as expected from the binding mode. However, the addition of a chlorine at position $R_4$ (compounds **44** and **47**) as well as the replacement of the methyl group by a chlorine atom or a trifluoromethyl moiety (compounds **45**, **46**, and **48**) was detrimental for binding affinity probably due mainly to steric effects, i.e., less favorable van der Waals interactions. Finally, compound **49** bearing methyl groups at positions $R_1$ and $R_5$ showed micromolar activity, reflecting that the introduction of an extra steric bulk on the molecule also decreases the binding affinity. As suggested by the similar hydrogen bonding pattern, compound **50** bearing an indazole ring displayed almost the same potency, at least in the FRET assay, as that of the original compound **3**.

In addition, the inhibition activity of our most potent compounds **3**, **40**, **43**, and **50** was assessed on Abl, Src, Lck, and Yes1 (Reaction Biology Corporation, Table 4). Compound **3** showed single digit nanomolar activity on Abl, Src, and Lck, while compounds **40**, **43**, and **50** retained high inhibition only on Src.

The six derivatives with nanomolar activity in the enzymatic assays (**40**, **41**, **43**, **45**, **48**, and **50**) were further evaluated in a

**Scheme 4.** [a,b]

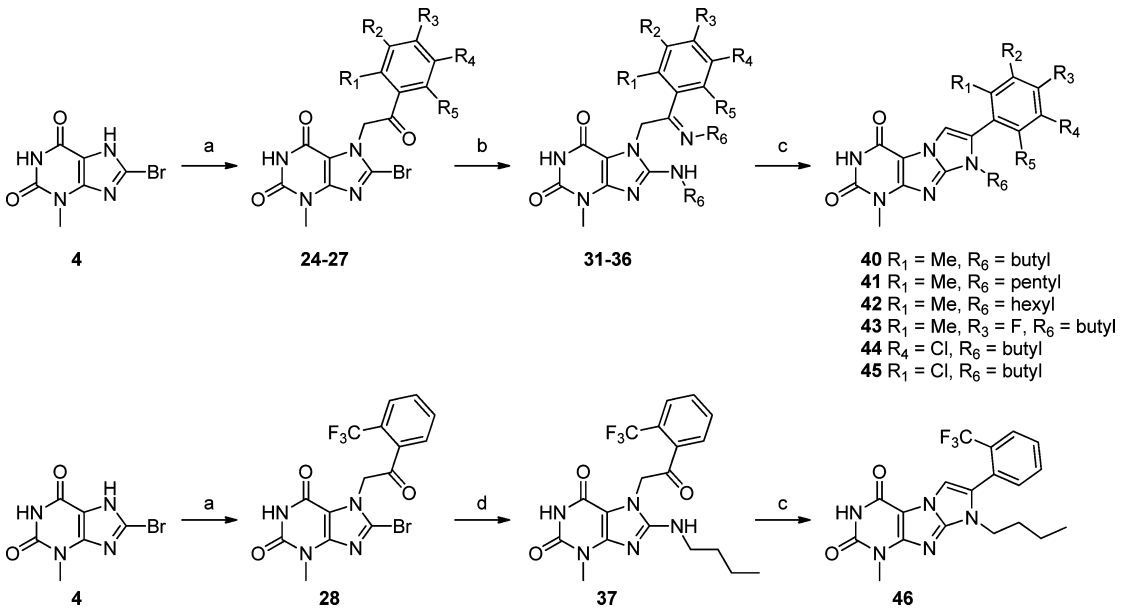


[a]Reagents and conditions: (a) $\alpha$-haloketone, DIPEA, DMF, 25 °C, 17 h. (b) Primary amine, sealed tube, 180 °C, 30 min. (c) $AlCl_3$, EtOH, sealed tube, 180 °C, 2–15 h. (d) Butylamine, EtOH, sealed tube, 180 °C, 1 h. [b]Unless otherwise stated, $R_n$ = H.


dx.doi.org/10.1021/jm301187e | J. Med. Chem. 2013, 56, 84–96

**Scheme 5.** [a,b]

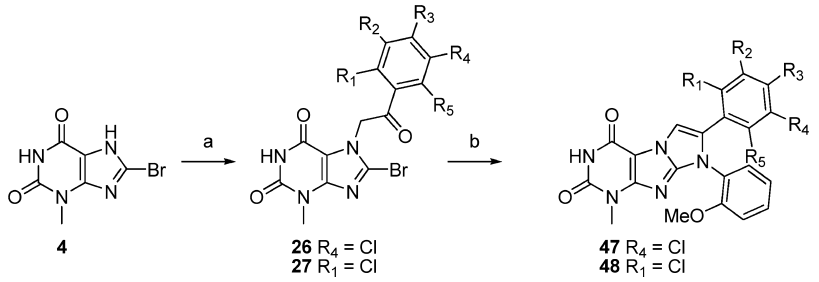


[a]Reagents and conditions: (a) α-haloketone, DIPEA, DMF, 25 °C, 17 h. (b) Anisidine, EtOH, sealed tube, reflux, 15 h. [b]Unless otherwise stated, $R_n$ = H.

**Scheme 6**[a]

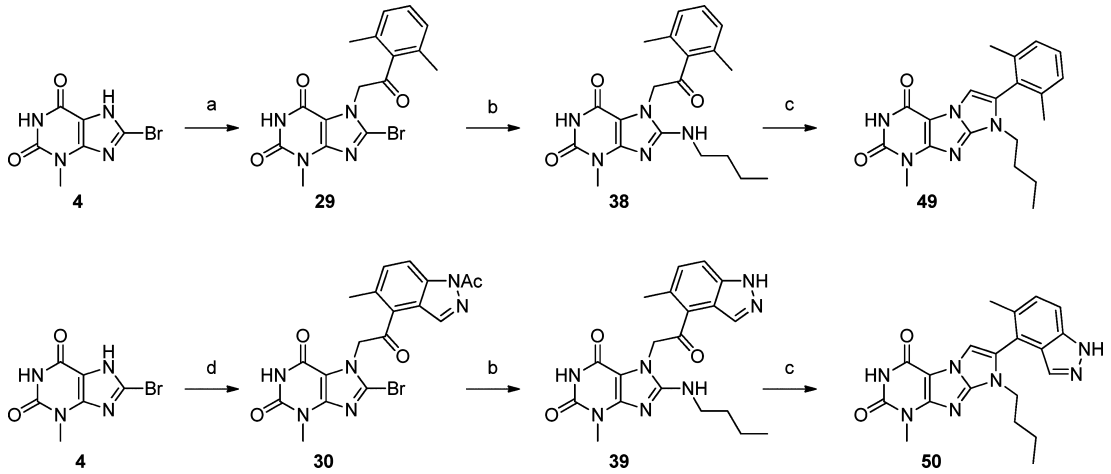


[a]Reagents and conditions: (a) 2-bromo-1-(2,6-dimethylphenyl)ethanone **18**, DIPEA, DMF, 110 °C, 2 h. (b) Butylamine, EtOH, sealed tube, 180 °C, 0.5−2 h. (c) $BF_3{\cdot}OEt_2$, DCM, sealed tube, 180 °C, 0.5−6 h. (d) KOH, EtOH, reflux, 2 h, then 1-(1-acetyl-5-methyl-1*H*-indazol-4-yl)-2-bromoethanone **19**, DMF, 110 °C, 2 h.

**Table 3. EphB4 Inhibition Data of Xanthine Derivatives**

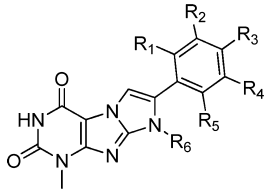

| | | | | | | | enzymatic assay $IC_{50}$ (nM) | | |
|---|---|---|---|---|---|---|---|---|---|
| compound | $R_1$ | $R_2$ | $R_3$ | $R_4$ | $R_5$ | $R_6$ | FRET[a] | radiometric[b] | cellular $IC_{50}$ (nM) |
| **40** | Me | H | H | H | H | butyl | 56 | 82 | 50 |
| **41** | Me | H | H | H | H | pentyl | 177 | n.d.[c] | 230 |
| **42** | Me | H | H | H | H | hexyl | 1300 | n.d. | n.d. |
| **43** | Me | H | F | H | H | butyl | 91 | 139 | 68 |
| **44** | H | H | H | Cl | H | butyl | 22% @ 10 μM | n.d. | n.d. |
| **45** | Cl | H | H | H | H | butyl | 182 | n.d. | 270 |
| **46** | $CF_3$ | H | H | H | H | butyl | 15% @ 10 μM | n.d. | n.d. |
| **47** | H | H | H | Cl | H | *o*-methoxyphenyl | 12% @ 10 μM | n.d. | n.d. |
| **48** | Cl | H | H | H | H | *o*-methoxyphenyl | 300 | n.d. | 2200 |
| **49** | Me | H | H | H | Me | butyl | 49% @ 10 μM | n.d. | n.d. |
| **50** | Me | H | H | indazole | | butyl | 14 | 133 | 150 |

[a]FRET-based enzymatic assay carried out using the Z′-LYTE Kinase Assay Kit−Tyr 1 Peptide (Invitrogen) following the vendor instructions. [b]Measured at Reaction Biology Corporation using radiolabeled ATP. [c]n.d.: not determined.

cellular phosphorylation assay on MEF cells transfected with myc-tagged human EphB4 (Proqinase, Table 3, right column). Except for compound **48** which showed micromolar affinity, the other five compounds displayed levels of inhibitory activity


dx.doi.org/10.1021/jm301187e | *J. Med. Chem.* 2013, 56, 84−96

Table 4. Abl, Lck, Src, and Yes1 Inhibition Data of Xanthine Derivatives[a]

| compound | Abl | Src | Lck | Yes1 |
|---|---|---|---|---|
| **3** | 0.92 | 1.14 | 1.3 | n.d.[b] |
| **40** | 578 | 71 | 493 | 284 |
| **43** | 1282 | 110 | 617 | 496 |
| **50** | 203 | 46 | 264 | 160.4 |

[a]Enzymatic assays were carried out at Reaction Biology Corporation using radiolabeled ATP. $IC_{50}$ values are given in nanomolar concentrations. [b]n.d.: not determined.

in the nanomolar range, which correlates with the potencies measured in the enzymatic assays. Of particular interest is the affinity of compounds **40** and **43**, with $IC_{50}$ values of 50 and 68 nM, respectively.

To further characterize this second generation of EphB4 inhibitors, the cell permeation of compounds **40** and **50** was evaluated on Caco-2 monolayers (Absorption Systems). Both compounds showed a high cell permeability; however, only compound **40** was not effluxed by transport proteins (Table 5), and thus it was selected for further evaluation in terms of selectivity (vide infra).

## SELECTIVITY PROFILE

To assess the selectivity profile of compound **40**, enzymatic assays were performed on a panel of 124 kinases (National Centre for Protein Kinase Profiling at the University of Dundee, Table 6, Figure 2, left, and Table S1 in the Supporting Information). In the presence of 3 $\mu$M concentration of compound **40**, only 5 of the 124 kinases tested (Src, Lck, EphA2, EphA4, and EphB2) had a remaining activity smaller than 10% with respect to a DMSO control. Furthermore, 5 other kinases (RIPK2, Yes1, EphB1, EphB3, and EphB4) showed a remaining activity between 10% and 20%. It is important to note that these 10 kinases have a threonine as a gatekeeper. Overall, compound **40** has a selectivity profile similar to that of **3**, with a strong inhibition of a relatively small fraction of the human kinome (Figure 2).

## ANTIPROLIFERATIVE ACTIVITY

Overexpression of the receptor tyrosine kinase EphB4 has been linked to several types of cancer, including breast,[26] colon,[27] and ovary.[28] To assess the potential of our inhibitors on a cancer model, compound **3** was submitted to the NCI-60 cancer cell line panel. Compound **3** displayed remarkable levels of cell growth inhibition against central nervous system (SNB-75, 128 nM), leukemia (K-562, 309 nM), and breast (HS 578T, 562 nM) cancer cells (data shown in the Supporting Information).

Table 6. Selectivity of Compound 40 Tested on a Panel of 124 Protein Kinases at the University of Dundee[a]

| kinase | % activity |
|---|---|
| MKK1 | 56 |
| RIPK2 | 12 |
| Src | 2 |
| Lck | 5 |
| CSK | 57 |
| Yes1 | 14 |
| Abl | 43 |
| BTK | 58 |
| Eph-A2 | 6 |
| Eph-A4 | 5 |
| Eph-B1 | 10 |
| Eph-B2 | 8 |
| Eph-B3 | 13 |
| Eph-B4 | 18 |

[a]The percentage of kinase activity is measured in the presence of 3 $\mu$M of **40** compared to a 100% DMSO control (only kinases with a percentage of activity below 70% are indicated). For full data set, see Table S1 in the Supporting Information.

In addition, the antiproliferative activity of compounds **3**, **40**, **41**, **43**, **45**, and **50** was assessed on patient-derived tumor cell lines using a propidium iodide-based proliferation assay and dasatinib as a reference (Oncotest, Table 7). Cell lines included colon, lung, kidney, pancreas, prostate, and stomach cancer cells. Overall, dasatinib exhibited the highest potency, with double-digit nanomolar activity against RXF 393NL, LXFA 983L, and PRXF DU145. Compounds **3**, **40**, **41**, **43**, **45**, and **50** inhibited cell proliferation in the low micromolar range, with compound **3** exhibiting good levels of antiproliferative activity against RXF 393NL, PAXF 1657L, and PRXF DU145. Compounds **45** and **50** displayed a 1−2 $\mu$M activity against the colon cancer cell line CXF 1103L. These results confirm the correlation between the kinase inhibitory activity of these molecules and their antiproliferative activity, although also reflect the need for further modifications to parallel the performance of "gold standards" in this field, such as dasatinib.

## CONFIRMATION OF THE BINDING MODE BY PROTEIN X-RAY CRYSTALLOGRAPHY

The binding mode of compounds **3**, **40**, and **50** was investigated by X-ray crystallography using the catalytic domain of EphA3 expressed in *E. coli*.[29] This tyrosine kinase was preferred to EphB4 for which only expression in insect cells has been reported. Note that 32 of the 36 residues in the ATP binding site of EphA3 are identical to those in EphB4.[30] Moreover, the side chains involved in binding compounds **3**, **40**, and **50** are identical in EphA3 and EphB4. These

Table 5. Cell Permeability Measurements for Compounds 3, 40, and 50 Using the Caco-2 Model

| | % recovery | | $P_{app}$ ($\times 10^{-6}$ cm/s)[a] | | | | |
|---|---|---|---|---|---|---|---|
| compound | A−B | B−A | A−B | B−A | efflux ratio[b] | permeability classification[c] | significant efflux[d] |
| **3** | 51 | 74 | 3.13 | 23.0 | 7.3 | high | yes |
| **40** | 85 | 89 | 42.7 | 28.1 | 0.7 | high | no |
| **50** | 84 | 96 | 8.02 | 49.0 | 6.1 | high | yes |

[a]Apparent permeability ($P_{app}$) is measured from the apical side to the basolateral side (A−B) and from the basolateral side to the apical side (B−A). [b]Efflux ratio = ($P_{app}$ B → A)/($P_{app}$ A → B). [c]Permeability classification: low = ($P_{app}$ A → B) < $1.0 \times 10^{-6}$cm/s; high = ($P_{app}$ A → B) > $1.0 \times 10^{-6}$ cm/s. [d]Significant efflux: efflux ratio > 3.0 and ($P_{app}$ B → A) > $1.0 \times 10^{-6}$ cm/s.


dx.doi.org/10.1021/jm301187e | J. Med. Chem. 2013, 56, 84−96

**Table 7. Antiproliferative Activity against Tumor Cell Lines**[a]

| Cell line | Origin | 3 | 40 | 41 | 43 | 45 | 50 | Dasatinib |
|---|---|---|---|---|---|---|---|---|
| CXF 1103L | Colon | 32.6 | 4.61 | 2.57 | 4.04 | 1.14 | 1.88 | 4.36 |
| GXF 251L | Gastric | 20.2 | 14.6 | 4.98 | 14.9 | 18.2 | 12.5 | 2.25 |
| LXFA 983L | Lung | 9.16 | 5.45 | 2.72 | 6.02 | 1.62 | 6.9 | 0.0565 |
| PAXF 1657L | Pancreas | 2.01 | 8.1 | 5.88 | 9.46 | 4.94 | 4 | 0.121 |
| PRXF DU145 | Prostate | 2.7 | 11.2 | 6.97 | 9.59 | 3.18 | 3.8 | 0.0623 |
| RXF 393NL | Renal | 1.76 | 7.6 | 5.58 | 8.69 | 2.93 | 2.63 | 0.0217 |
| Geomean $IC_{50}$ | | 6.21 | 7.96 | 4.47 | 8.11 | 3.40 | 4.32 | 0.212 |

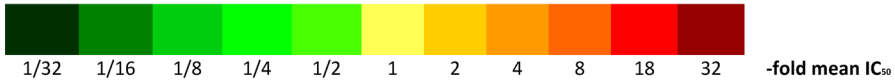


[a] $IC_{50}$ values were determined at Oncotest using a modified propidium iodide assay. Measurements were performed after 4 days of incubation with the corresponding compound. $IC_{50}$ values are given in micromolar concentrations ($\mu$M).

observations explain the very similar potency on both targets of our inhibitors and other Eph kinase inhibitors reported previously.[6]

Crystals were obtained using the hanging drop vapor diffusion method (see Experimental Section). The final resolution is 2.2 Å, 1.9 Å, and 2.1 Å for the complexes of EphA3 with compounds **3**, **40**, and **50**, respectively; further details of refinement statistics are shown in Table 8.

Strikingly, the binding mode of compound **3** observed in the crystal structure is essentially identical to that predicted by docking and explicit solvent molecular dynamics[6] (Figure 3). The pyrimidine ring is involved in two hydrogen bonds with the hinge region, and the phenol moiety is nestled into the so-called back pocket with its hydroxyl group accepting a hydrogen bond from the backbone NH of Asp758 (Asp764 for EphA3) of the DFG loop and donating a hydrogen bond to the side chain of Glu664 (Glu670 for EphA3) (Figure 1, right).

Superposition of the crystal structures obtained for compounds **3**, **40** and **50** shows that the key features of the binding mode are conserved, such as the hydrogen bond interactions between the pyrimidine ring and Met702, as well as the orientation of the phenyl ring in the back pocket (Figure 4). Interestingly, the indazole ring of compound **50** is involved in two hydrogen bond interactions: the NH group acts as donor to the Glu670 side chain, and the imine nitrogen acts as acceptor for the backbone NH of Asp764. The methoxy group of compound **3** matches the butyl side chains of compounds **40** and **50**, as both of these substituents point in the opposite direction of the hinge region. An in-depth comparative analysis of the binding modes of compounds **3**, **40**, and **50**, with the X-ray structures of two other series of EphB4/A3 inhibitors discovered in our groups as well as with the inhibitor/Eph complexes available in the PDB database, will be published elsewhere (Jing Dong et al., in preparation).

Finally, the binding mode of compound **3**, predicted and validated as belonging to type $I_{1/2}$,[6,7] lends itself to a modification into type II[3,8] via replacement of the hydroxyl group by an amide linker and addition of an aromatic group, e.g., $CF_3$-substituted benzol, to reach the so-called allosteric site proximal to the ATP binding site. We are currently planning the synthesis of these type II derivatives.

**Table 8. X-ray Data Collection**

| | 3 | 40 | 50 |
|---|---|---|---|
| space group | P 1 21 1 | P 1 21 1 | P 1 21 1 |
| unit cell | | | |
| *a* (Å) | 52.6 | 53.29 | 53.06 |
| *b* (Å) | 38.2 | 38.25 | 38.18 |
| *c* (Å) | 75.7 | 76.04 | 75.84 |
| resolution range (Å) | 38.2−2.2 | 34.0−1.9 | 38.2−2.1 |
| unique reflections | 15076 (2090) | 23747 (3297) | 17532 (2402) |
| $\langle I/\sigma(I)\rangle$ | 8.8 (3.0) | 8.9 (2.8) | 10.6 (3.9) |
| *R* merge | 0.103 (0.457) | 0.084 (0.405) | 0.086 (0.334) |
| completeness (%) | 98.4 (94.6) | 98.5 (94.8) | 98.8 (93.4) |
| multiplicity | 3.7 (3.5) | 3.0 (2.9) | 3.5 (3.4) |
| refinement | | | |
| resolution range (Å) | 30.68−2.20 | 29.79−1.90 | 29.70−2.10 |
| *R* factor/*R* free | 19.15/23.25 | 18.45/22.34 | 17.37/22.53 |
| mean *B* factors (Å$^2$) | 30.8 | 24.3 | 28.8 |
| RMS bonds (Å) | 0.0077 | 0.0071 | 0.0071 |
| RMS angles (deg) | 1.505 | 1.377 | 1.365 |

## CONCLUSIONS

Recently, a medicinal chemistry campaign inspired by the pose of the original hit obtained by docking resulted in the discovery of compound **3**, a single-digit nanomolar inhibitor of the EphB4 tyrosine kinase. However, further evaluation of compound **3** revealed a major discrepancy between enzymatic and cellular activity (5 nM in enzymatic assay vs 130 nM in cellular phosphorylation assay). Furthermore, efficient efflux by P-glycoprotein transporters was observed on caco-2 monolayers.

Aided by the docked pose of compound **3**, a second generation of EphB4 inhibitors was designed and synthesized to


dx.doi.org/10.1021/jm301187e | J. Med. Chem. 2013, 56, 84−96

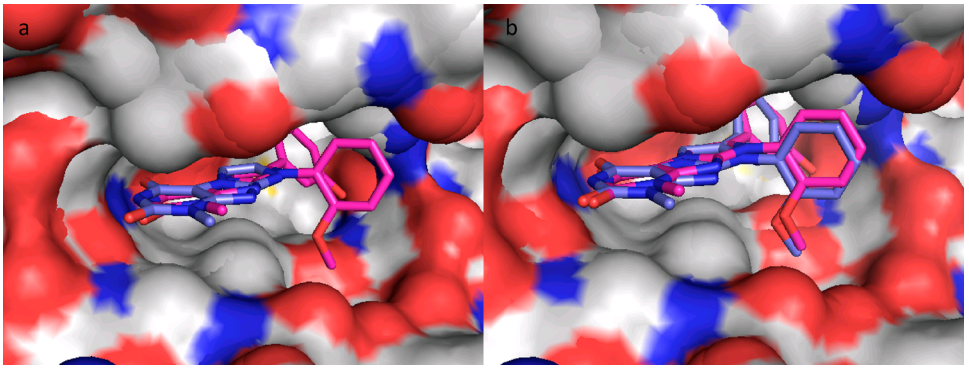


**Figure 3.** Comparison of docking results with the X-ray structure. (a) Superposition of the X-ray structure of the complex of EphA3 with compound **3** (magenta C atoms) and the pose of its anchor fragment (blue C atoms) as predicted by docking into EphB4. (b) Superposition of the X-ray structure of the complex of EphA3 with compound **3** (magenta C atoms) and the binding mode into EphB4 obtained by explicit solvent molecular dynamics (blue C atoms). The coloring scheme of the protein surface (shown only for EphA3) emphasizes donor/acceptor (blue/red) and hydrophobic (white). The residues in the ATP binding site of EphA3 and EphB4 are identical.

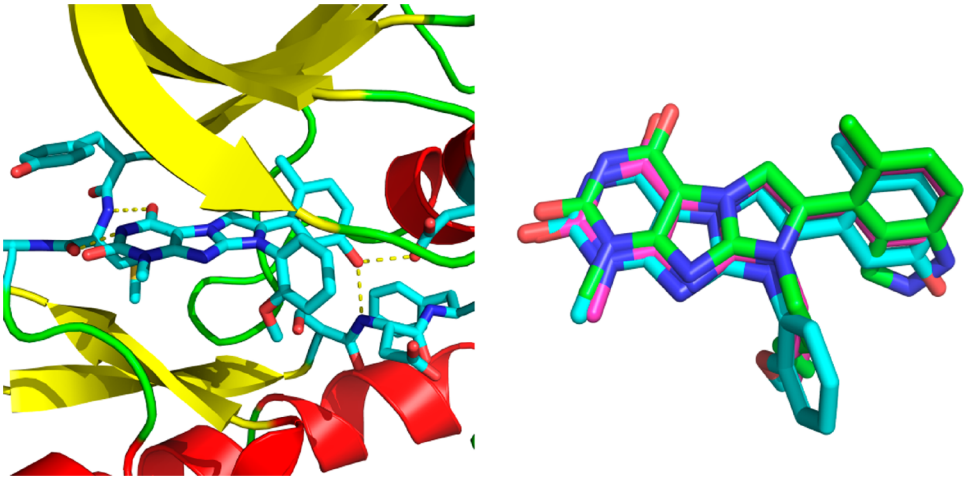

**Figure 4.** (a) X-ray structure of compound **3** (carbon atoms in cyan) in complex with EphA3. (b) Superposition of compounds **3** (carbon atoms in cyan), **40** (magenta C atoms), and **50** (green C atoms).

address this dichotomy. Among this small library of carefully tailored molecules, compound **40** showed a 50 nM inhibition activity both in enzymatic and cell-based assays. Further biological analysis suggested that compound **40** was not actively effluxed, thus improving the pharmacological properties compared to the previous series. In addition, strong inhibition activity was observed on only 5% of a 124 kinase panel which shows that compound **40** has a selectivity profile as good as that of compound **3**.

Remarkably, the binding mode of compounds **3**, **40**, and **50** suggested by docking followed by MD simulations with explicit solvent has been confirmed by X-ray crystallography. In particular, there is a perfect overlap with the crystal structure for the important features of the predicted binding mode of compounds **3**, **40**, and **50**, such as the hydrogen bonding pattern with the hinge region and the orientation of the phenyl or indazole ring in the back pocket.

In summary, further synthetic efforts and additional biochemical profiling provided new EphB4 tyrosine kinase inhibitors with improved activity in cellular assays. Thus, compound **40** holds promise for further evaluation in in vivo models.

## EXPERIMENTAL SECTION

**Chemistry.** All reactions, unless otherwise stated, were carried out under a nitrogen atmosphere using standard Schlenk techniques. All reagents were used as received unless otherwise noted. Solvents were purchased in the best quality available, degassed by purging thoroughly with nitrogen, and dried over activated molecular sieves of appropriate size. Alternatively, they were purged with argon and passed through alumina columns in a solvent purification system (Innovative Technology). Reactions were monitored by thin layer chromatography (TLC) using Merck TLC silica gel 60 F254. Flash column chromatography was performed over silica gel (230−400 mesh). NMR spectra were recorded on AV2 400 or AV2 500 MHz Bruker spectrometers. Chemical shifts are given in ppm. The spectra are calibrated to the residual $^{1}H$ and $^{13}C$ signals of the solvents. Multiplicities are abbreviated as follows: singlet (s), doublet (d), triplet (t), quartet (q), doublet−doublet (dd), quintet (quint), septet (sept), multiplet (m), and broad (br). Melting points were determined on a Büchi Melting Point B-540 instrument. 4-Fluoro-2-methylbenzaldehyde (**5**), 2-bromo-1,3-dimethylbenzene (**8**), 2′-chloroacetophenone (**14**), 3′-chloroacetophenone (**15**), and 2′-(trifluoromethyl)-acetophenone (**16**) were purchased from Fluka. 2-Bromo-1-(*o*-tolyl)ethanone (**23**) was purchased from Synchem. Compounds **1**−**4** have been previously described.[6]

High-resolution electrospray ionization mass spectrometry was performed on a Finnigan MAT 900 (Thermo Finnigan, San Jose, CA) double-focusing magnetic sector mass spectrometer. Ten spectra were acquired. A mass accuracy ≤2 ppm was obtained in the peak-matching


dx.doi.org/10.1021/jm301187e | *J. Med. Chem.* 2013, 56, 84−96

acquisition mode by using a solution containing 2 μL of PEG200, 2 μL of PPG450, and 1.5 mg of NaOAc (all obtained from Sigma-Aldrich, Buchs, Switzerland) dissolved in 100 mL of MeOH (HPLC Supra grade, Scharlau, E-Barcelona) as internal standard. The purity of all tested compounds was determined by HPLC on a Waters Acquity UPLC (Waters, Milford, MA) Top spectrometer using an Acquity BEH C18 HPLC column (1.7 μm, 1 × 50 mm, Waters) with a mixture of $H_2O$ + 0.1% HCOOH (A) and $CH_3CN$ + 0.1% HCOOH (B) solvent (0.1 mL flow rate, linear gradient from 5% to 98% B within 4 min followed by flushing with 98% B for 1 min). UV detection was set to 200−260 nm. Unless otherwise stated, all the compounds showed ≥95% purity.

**General Procedure for the α-Bromination of Acetophenones.** A solution of the acetophenone (1 equiv) in $CHCl_3$ (0.18 M) was added to a refluxing solution of copper(II) bromide (1.99 equiv) in EtOAc (0.45 M). The mixture was then refluxed for 10 h. The solution was filtered through Celite and concentrated under reduced pressure to afford a green solid. The solid was purified by flash chromatography on silica gel to afford the corresponding products in pure form. This method was used to obtain compounds **17**−**22**. 2-Bromo-1-(*o*-tolyl)ethanone (**23**) was purchased from Synchem.

**General Procedure for the Preparation of Alkylated Xanthines.** 3-Methyl-8-bromoxanthine (**4**, 1 equiv) was dissolved in DMF (0.4 M), and *N*,*N*-diisopropylethylamine (1.5 equiv) was added. After the mixture was stirred for 5 min at 25 °C, α-bromoacetophenone (1 equiv) was added. The reaction was stirred at 25 °C for 15 h. The mixture was then concentrated under reduced pressure, methanol was added, and the formed precipitate was filtered off and washed with water to afford the corresponding product in pure form. This method was used to obtain compounds **24**−**28**.

**General Procedure A for the Cyclization of Alkylated Xanthines.** A mixture of 3-alkyl-8-bromo-3,7-dihydro-7-(2-oxo-2-phenylethyl)-1*H*-purine-2,6-dione (1.0 equiv) and alkylamine (0.1 M) was heated in a sealed tube at 180 °C for 30 min. The reaction was cooled to room temperature and evaporated to dryness. The resulting residue was triturated with a mixture acetone/water, and the precipitate was filtered off. The crude intermediate was heated in a sealed tube at 180 °C in EtOH (0.1 M) in the presence of $AlCl_3$ (2 equiv) for 2−15 h. The reaction was poured into water and extracted with $CH_2Cl_2$, and the organic layer was dried over $MgSO_4$, filtered, and concentrated under reduced pressure. Purification by column chromatography on silica gel ($CH_2Cl_2$/EtOAc 1:1) afforded the corresponding product in pure form. This method was used to obtain intermediates **31**−**36** and final products **40**−**45**.

**General Procedure B for the Cyclization of Alkylated Xanthines.** A mixture of 3-alkyl-8-bromo-3,7-dihydro-7-(2-oxo-2-phenyl-ethyl)-1*H*-purine-2,6-dione (1.0 equiv) and the anisidine (4.0 equiv) in EtOH (concentration, 0.1 M) was heated in a sealed tube at 180 °C for 12 h. The reaction was cooled to room temperature, and the formed solid was filtered off and washed with water to afford the corresponding product in pure form. This method was used to obtain compounds **47** and **48**.

**Synthesis of Compound 40.** *8-Bromo-3-methyl-7-(2-oxo-2-(o-tolyl)ethyl)-1H-purine-2,6(3H,7H)-dione (**24**).* White solid; yield: 58%; $^1$H NMR (500 MHz, DMSO-$d_6$): δ = 11.32 (s, 1H), 8.04 (dd, *J* = 7.6 Hz, *J* = 1.1 Hz, 1H), 7.56 (dt, *J* = 7.6 Hz, *J* = 1.1 Hz, 1H), 7.44 (t, *J* = 7.6 Hz, 1H), 7.40 (d, *J* = 7.6 Hz, 1H), 5.79 (s, 2H), 3.37 (s, 3H), 2.42 (s, 3H); HRMS (ESI): *m*/*z*: calcd for $C_{15}H_{13}BrN_4O_3Na^+$: 399.0069, found: 399.0068.

*8-(Butylamino)-7-(2-(butylimino)-2-(o-tolyl)ethyl)-3-methyl-1H-purine-2,6(3H,7H)-dione (**31**).* White solid; $^1$H NMR (500 MHz, DMSO-$d_6$): δ = 10.53 (s, 1H), 7.31−7.25 (m, 4H), 6.90 (t, *J* = 5.6 Hz, 1H), 4.98 (d, *J* = 18.2 Hz, 1H), 4.85 (d, *J* = 18.2 Hz, 1H), 3.33 (s, 2H), 3.29 (s, 3H), 3.03−2.98 (m, 1H), 2.83−2.78 (m, 1H), 2.17 (s, 3H), 1.57−1.51 (m, 2H), 1.39−1.32 (m, 2H), 1.28−1.23 (m, 2H), 1.16−1.00 (m, 2H), 0.91 (t, *J* = 7.3 Hz, 3H), 0.69 (t, *J* = 7.3 Hz, 3H); HRMS (ESI): *m*/*z*: calcd for $C_{23}H_{32}N_6O_2H^+$: 425.2660, found: 425.2661.

*8-Butyl-1-methyl-7-(o-tolyl)-1H-imidazo[2,1-f]purine-2,4(3H,8H)-dione (**40**).* White solid; yield: 32% over two steps; mp 258−260 °C; $^1$H NMR (500 MHz, DMSO-$d_6$): δ = 10.94 (s, 1H), 7.62 (s, 1H), 7.46−7.33 (m, 4H), 3.82 (t, *J* = 7.3 Hz, 2H), 3.40 (s, 3H), 2.24 (s, 3H), 1.54 (quint, *J* = 7.3 Hz, 2H), 1.06 (sext, *J* = 7.3 Hz, 2H), 0.68 (t, *J* = 7.3 Hz, 3H); HRMS (ESI): *m*/*z*: calcd for $C_{19}H_{21}N_5O_2Na^+$: 374.1588, found: 374.1585.

**Synthesis of Compound 46.** *8-Bromo-3-methyl-7-(2-oxo-2-(2-(trifluoromethyl)phenyl)ethyl)-1H-purine-2,6(3H,7H)-dione (**28**).* White solid; yield: 54%; $^1$H NMR (500 MHz, DMSO-$d_6$): δ = 11.41 (s, 1H), 8.09 (d, *J* = 7.5 Hz, 1H), 7.96−7.92 (m, 2H), 7.87−7.84 (m, 1H), 5.78 (s, 2H), 3.36 (s, 3H); HRMS (ESI): *m*/*z*: calcd for $C_{15}H_{10}BrF_3N_4O_3H^+$: 430.9961, found: 430.9963.

*8-(Butylamino)-3-methyl-7-(2-oxo-2-(2-(trifluoromethyl)phenyl)-ethyl)-1H-purine-2,6(3H,7H)-dione (**37**).* A mixture of 8-bromo-3-methyl-7-(2-oxo-2-(2-(trifluoromethyl)phenyl)ethyl)-1*H*-purine-2,6-(3*H*,7*H*)-dione (**28**, 490 mg, 1.13 mmol) and butylamine (0.448 mL, 4.55 mmol) in EtOH (11 mL) was heated in a sealed tube at 180 °C for 1 h. The reaction was cooled to room temperature, and the solid was filtered off to afford the crude product as a light yellow solid (345 mg, 74% yield). $^1$H NMR (500 MHz, DMSO-$d_6$): δ = 10.62 (s, 1H), 8.15 (d, *J* = 7.6 Hz, 1H), 7.94−7.89 (m, 2H), 7.85−7.82 (m, 1H), 7.03 (t, *J* = 5.4 Hz, 1H), 5.55 (s, 2H), 3.32 (s, 3H), 1.53 (quint, *J* = 7.3 Hz, 2H), 1.33 (sext, *J* = 7.3 Hz, 2H), 0.90 (t, *J* = 7.3 Hz, 3H), 3.31 (s, 2H); HRMS (ESI): *m*/*z*: calcd for $C_{19}H_{20}F_3N_5O_3H^+$: 424.1591, found: 424.1593.

*8-Butyl-1-methyl-7-(2-(trifluoromethyl)phenyl)-1H-imidazo[2,1-f]purine-2,4(3H,8H)-dione (**46**).* 8-(Butylamino)-3-methyl-7-(2-oxo-2-(2-(trifluoromethyl)phenyl)ethyl)-1*H*-purine-2,6(3*H*,7*H*)-dione (**37**, 345 mg, 0.81 mmol) was heated in a sealed tube at 180 °C in EtOH (8 mL) in the presence of $AlCl_3$ (543 mg, 4.07 mmol) for 15 h. The reaction was poured in water and extracted with $CH_2Cl_2$, and the organic layer was dried over $MgSO_4$, filtered, and concentrated under reduced pressure. Purification by column chromatography on silica gel ($CH_2Cl_2$/EtOAc 1:1) afforded the desired compound as a white solid (50 mg, 15% yield). mp 267−269 °C; $^1$H NMR (500 MHz, DMSO-$d_6$): δ = 10.98 (s, 1H), 7.98 (d, *J* = 7.4 Hz, 1H), 7.87 (t, *J* = 7.4 Hz, 1H), 7.81 (t, *J* = 7.4 Hz, 1H), 7.77 (d, *J* = 7.4 Hz, 1H), 7.63 (s, 1H), 3.81 (t, *J* = 7.3 Hz, 2H), 3.40 (s, 3H), 1.56 (quint, *J* = 7.3 Hz, 2H), 1.13 (sext, *J* = 7.3 Hz, 2H), 0.72 (t, *J* = 7.3 Hz, 3H); HRMS (ESI): *m*/*z*: calcd for $C_{19}H_{18}F_3N_5O_2H^+$: 406.1485, found: 406.1483.

**Synthesis of Compound 50.** *7-(2-(1-Acetyl-5-methyl-1H-indazol-4-yl)-2-oxoethyl)-8-bromo-3-methyl-1H-purine-2,6(3H,7H)-dione (**30**).* 8-Bromo-3,9-dihydro-3-methyl-1*H*-purine-2,6-dione (**4**, 250 mg, 1.02 mmol) was added to a solution of KOH (57 mg, 1.02 mmol) in EtOH (3 mL). The resulting mixture was then heated to reflux for 2 h. EtOH was then removed under reduced pressure, and the resulting solid was washed with cold EtOH, and filtered off to afford a light yellow solid. A mixture of this solid (144 mg, 0.51 mmol) was dissolved in DMF (1.3 mL), and 1-(1-acetyl-5-methyl-1*H*-indazol-4-yl)-2-bromoethanone (**19**, 150 mg, 0.51 mmol) was added to the mixture. The reaction was stirred at 110 °C for 2 h. The mixture was then concentrated under reduced pressure, methanol was added, and the formed precipitate was filtered off and washed with water to afford the product as a light yellow solid (184 mg, 39% yield over two steps). $^1$H NMR (500 MHz, DMSO-$d_6$): δ = 11.48 (s, 1H), 8.64 (d, *J* = 0.7 Hz, 1H), 8.42 (d, *J* = 8.7 Hz, 1H), 7.65 (d, *J* = 8.7 Hz, 1H), 5.84 (s, 2H), 3.39 (s, 3H), 2.75 (s, 3H), 2.53 (s, 3H); HRMS (ESI): *m*/*z*: calcd for $C_{18}H_{15}BrN_6O_4H^+$: 459.0411, found: 459.0407.

*8-(Butylamino)-3-methyl-7-(2-(5-methyl-1H-indazol-4-yl)-2-oxoethyl)-1H-purine-2,6(3H,7H)-dione (**39**).* A mixture of 7-(2-(1-acetyl-5-methyl-1*H*-indazol-4-yl)-2-oxoethyl)-8-bromo-3-methyl-1*H*-purine-2,6(3*H*,7*H*)-dione (**30**, 143 mg, 0.31 mmol) and butylamine (0.123 mL, 1.24 mmol) in EtOH (3 mL) was heated in a sealed tube at 175 °C for 30 min. The reaction was cooled to room temperature, and the solid was filtered off to afford the crude product as a light yellow solid (120 mg, 93% yield). $^1$H NMR (500 MHz, DMSO-$d_6$): δ = 13.35 (s, 1H), 10.70 (s, 1H), 8.46 (s, 1H), 7.68 (d, *J* = 8.5 Hz, 1H), 7.34 (d, *J* = 8.5 Hz, 1H), 7.09 (t, *J* = 5.1 Hz, 1H), 5.57 (s, 2H), 3.34 (s, 5H), 2.47 (s, 3H), 1.55 (quint, *J* = 7.3 Hz, 2H), 1.36 (sext, *J* = 7.3 Hz, 2H), 0.91 (t, *J* = 7.3 Hz, 3H); HRMS (ESI): *m*/*z*: calcd for $C_{20}H_{23}N_7O_3H^+$: 410.1935, found: 410.1937.


dx.doi.org/10.1021/jm301187e | J. Med. Chem. 2013, 56, 84−96

*8-Butyl-1-methyl-7-(5-methyl-1H-indazol-4-yl)-1H-imidazo[2,1-f]purine-2,4(3H,8H)-dione (**50**).* 8-(Butylamino)-3-methyl-7-(2-(5-methyl-1*H*-indazol-4-yl)-2-oxoethyl)-1*H*-purine-2,6(3*H*,7*H*)-dione (**39**, 40 mg, 0.09 mmol) was heated in a sealed tube at 175 °C in $CH_2Cl_2$ (4 mL) in the presence of $BF_3{\cdot}OEt_2$ (0.4 mL, 3.24 mmol) for 30 min. The reaction was poured in water and extracted with $CH_2Cl_2$, and the organic layer was dried over $MgSO_4$, filtered, and concentrated under reduced pressure. Purification by column chromatography on silica gel (gradient EtOAc:MeOH 99:1 to 98:2) afforded the desired compound as a white solid (1.1 mg, 3% yield). $^1$H NMR (400 MHz, DMSO-$d_6$): $\delta$ = 13.21 (s, 1H), 10.93 (s, 1H), 7.83 (s, 1H), 7.69 (s, 1H), 7.63 (d, $J$ = 8.5 Hz, 1H), 7.39 (d, $J$ = 8.5 Hz, 1H), 3.77 (t, $J$ = 7.3 Hz, 2H), 3.43 (s, 3H), 2.31 (s, 3H), 1.48 (quint, $J$ = 7.3 Hz, 2H), 0.98 (sext, $J$ = 7.3 Hz, 2H), 0.55 (t, $J$ = 7.3 Hz, 3H); HRMS (ESI): $m/z$: calcd for $C_{20}H_{21}N_7O_2Na^+$: 414.1649, found: 414.1646.

**FRET-Based Enzymatic Assay.** Compounds were tested in the Z′-LYTE Kinase Assay Kit−Tyr 1 Peptide (Invitrogen, USA) in a Corning 384 well microtiter plate. Fluorescence progress curves were measured upon excitation at 400 nm and emission at 445 and 520 nm. The assay contained a final concentration of EphB4 and ATP of 25 ng/$\mu$L and 125 $\mu$M (which is near its $K_m$), respectively, and was run at room temperature for 2 h. $IC_{50}$ values (inhibitor concentration at which enzyme activity is reduced by 50%) are determined after carrying out assays at 10 different concentrations between 20 $\mu$M and 10 pM.

**[$\gamma$-33P]ATP-Based Enzymatic Assay.** The enzymatic assays for the selectivity profile were performed at the National Centre for Protein Kinase Profiling at the University of Dundee. All assays (25.5 $\mu$L volume) were carried out robotically at room temperature and were linear with respect to time and enzyme concentration under the conditions used. Assays were performed for 30 min using Multidrop Micro reagent dispensers (Thermo Electron Corporation, Waltham, MA) in a 96-well format. The concentration of magnesium acetate in the assays was 10 mM and [$\gamma$-$^{33}$P]ATP (800 cpm/pmol) was used at 5, 20, or 50 $\mu$M to be at or below the $K_m$ for ATP for each kinase. The assays were initiated with MgATP, stopped by the addition of 5 $\mu$L of 0.5 M orthophosphoric acid, and spotted onto P81 filter plates using a unifilter harvester (PerkinElmer, Boston, MA). The data is presented as mean percentage activity of duplicate assays at single concentration compared to DMSO controls. A similar protocol was used at Reaction Biology Corporation to measure the inhibitory activity of compounds **3**, **40**, **43**, and **50** against Abl, Src, Lck, and Yes1.

**Cellular Phosphorylation Assays.** The following experiments were performed at ProQinase GmbH. Mouse embryonal fibrablast cells, stably transfected to overexpress full-length human EphB4, were plated at $4 \times 10^4$ cells/well in DMEM supplemented with 10% FCS in 48-well culture dishes. Medium was replaced by DMEM without FCS before test compounds prediluted in 100% DMSO were added (final DMSO concentration of 1%). After incubation for 90 min at 37 °C, cells were stimulated for 2 h at 4 °C using murine ephrinB2-Fc at a final concentration of 2 $\mu$g/mL. Quantification of EphB4 phosphorylation was assessed in a 96-well plate via sandwich ELISA using a myc capture antibody and an antiphosphotyrosine detection antibody.

**Cellular Permeability Assays.** The following experiments were performed at Absorption Systems. Caco-2 monolayers were grown to confluence on collagen-coated, microporous, polycarbonate membranes in 12-well Costar Transwell plates. The permeability assay buffer for the donor chambers was Hanks Balanced Salt Solution containing 10 mM HEPES and 15 mM glucose at a pH of 7.4. The buffer in the receiver chambers also contained 1% bovine serum albumin. Cells were dosed on the apical side (A-to-B) or basolateral side (B-to-A) and incubated at 37 °C with 5% $CO_2$ in a humidified incubator. After 2 h, aliquots were taken from the donor and receiver chambers. Each determination was performed in duplicate. The flux of lucifer yellow was also measured for each monolayer after being subjected to the test compounds to ensure that no damage was inflicted to the cell monolayers during the flux period. All samples were assayed by LC-MS/MS using electrospray ionization. The apparent permeability, $P_{app}$, and percent recovery were calculated as follows:

$$P_{app} = (dC_r/dt) \times V_r/(A \times C_A) \quad (1)$$

$$\text{percent recovery} = 100 \times ((V_r \times C_r^{\text{final}}) + (V_d \times C_d^{\text{final}}))/(V_d \times C_0) \quad (2)$$

where, $dC_r/dt$ is the slope of the cumulative concentration in the receiver compartment versus time in $\mu M{\cdot}s^{-1}$, $V_r$ is the volume of the receiver compartment in $cm^3$, $V_d$ is the volume of the donor compartment in $cm^3$, $A$ is the area of the cell monolayer (1.13 $cm^2$ for 12-well Transwell), $C_0$ is the nominal concentration of the dosing solution in micromolar, $C_A$ is the average of the nominal concentration of the dosing solution and the measured donor concentration at 120 min in $\mu$M, $C_r^{\text{final}}$ is the cumulative receiver concentration in micromolar at the end of the incubation period, and $C_d^{\text{final}}$ is the concentration of the donor in micromolar at the end of the incubation period.

**Monolayer Assay.** Cell lines were routinely passaged once or twice weekly and maintained in culture for up to 20 passages. All cells were cultured in RPMI 1640 medium supplemented with 10% (v/v) fetal calf serum and 0.1 mg/mL gentamicin (medium and all components from PAA, Cölbe, Germany) at 37 °C in a humidified atmosphere with 5% $CO_2$.

A modified propidium iodide (PI) assay was used to assess the anticancer activity of the compounds. Briefly, cells were harvested from exponential phase cultures, counted, and plated in 96-well flat-bottom microtiter plates at a cell density of 4000−20 000 cells per well. After a 24 h recovery period, allowing the cells to resume exponential growth, 10 $\mu$L of culture medium (four control wells/plate) and culture medium with the test compound were added by the liquid handling robotic system and treatment was continued for four days. The compounds were applied in half log increments at 10 concentrations in duplicate. Next, cells were washed with 200 $\mu$L of PBS to remove dead cells. Subsequently, 200 $\mu$L of a solution containing 7 $\mu$g/mL propidium iodide (PI) and 0.1% (v/v) Triton X-100 was added. After an incubation period of 1−2 h at room temperature, fluorescence (FU) was measured using the Cytofluor 4000 microplate reader (excitation $\lambda$ = 530 nm, emission $\lambda$ = 620 nm) to quantify the amount of attached viable cells. For calculations, the mean value of duplicate/quadruplicate (untreated control) data was used. Quality criteria for a successful assay included fluorescence intensity signal of >500 units from the untreated control wells.

**X-ray Crystallography.** The atomic coordinates and structure factors of EphA3 in complex with the inhibitors **3**, **40**, and **50** have been deposited with the Protein Data Bank as entries 4GK2, 4GK3, and 4GK4, respectively.

*Protein Expression and Purification.* A clone of the EphA3 kinase domain (residues: 606−947) was obtained from Prof. Sirano Dhe-Paganon's group[29] and expressed in *E. coli* strain BL21 (DE3). Cells expressing EphA3 were induced with a 1 mM solution of isopropyl $\beta$-D-thiogalactopyranoside (IPTG) for 12 h at 15 °C. Cell pellets were resuspended in buffer A (50 mM Tris, pH 8.0, and 100 mM NaCl, supplemented with protease inhibitors) and lysed by sonication. After centrifugation at 15 000 rpm for 1 h, the soluble fraction of EphA3 was purified using HisTrap FF crude and HiTrap Q HP columns (GE Healthcare), followed by gel filtration chromatography (Superdex75; GE Healthcare). The appropriate fractions were combined and concentrated to ∼10 mg/mL using Amicon filter devices (10 kDa as cutoff) in a storage solution (100 mM sodium chloride and 10 mM Tris-HCl pH 8.0, 5% glycerol). The resulting solution was aliquoted and stored at −80 °C for further usage.

*Crystallization, Data Collection, and Structure Determination.* Crystals of the EphA3 kinase domain were grown at 20 °C using the hanging drop vapor diffusion method. Equal volumes of protein and reservoir solutions (0.1 M sodium cacodylate pH 6.5, 0.15 M ammonium sulfate, 22.5% PEG 3350) were mixed, and crystals appeared after 1 to 2 days. A 5 mM solution of inhibitor (in 100% DMSO) was added to the hanging drop to reach a final DMSO concentration of 10% (v/v). The crystals were soaked for 1 to 24 h and flash-frozen in liquid nitrogen without extra cryoprotectant.


dx.doi.org/10.1021/jm301187e | J. Med. Chem. 2013, 56, 84−96

Data sets were collected on a MarCCD detector and indexed, integrated, and scaled with the XDS[31] and CCP4 programs.[32] The structures were solved by molecular replacement with PHASER[33] using the apo EphA3 kinase domain structure (PDB entry 2GSF) as a search model and refined with PHENIX.[34]

The Simulated Annealing Composite OMIT map (Supporting Information), in which compound **3** was omitted from structure factor calculation, was generated in a region within 1.6 Å of compound **3** using PHENIX and Pymol (http://www.pymol.org).

## ■ ASSOCIATED CONTENT

### Supporting Information

Selectivity data of compound **40**, antiproliferative activity of compound **3**, $^{1}$H NMR and $^{13}$C NMR of selected compounds, and HPLC traces (for purity) of tested compounds and simulated annealing composite OMIT map. This material is available free of charge via the Internet at http://pubs.acs.org.

## ■ AUTHOR INFORMATION


### Corresponding Author

*Phone: (41) 446353945. Fax: (41) 446353948. E-mail: nevado@oci.uzh.ch, caflisch@bioc.uzh.ch.

### Author Contributions

#These two authors contributed equally to this work.


### Notes

The authors declare no competing financial interest.

## ■ ACKNOWLEDGMENTS

We are grateful to Maja Bollhalder, the late Sara Savaresi, Sabrina Sonda, and Changchuan Xie for technical help in a preliminary phase of this work. We also thank Xiao-Dan Li and Chitra Rajendran for interesting discussions and help with data collection. Prof. Sirano Dhe-Paganon is kindly acknowledged for providing the plasmid for EphA3 expression. This work was supported financially in part by a grant of the Sino-Swiss program to A.C. and by the Forschungskredit of the University of Zürich to K.L.

## ■ ABBREVIATIONS: USED

Abl, abelson murine leukemia viral oncogene homologue; ATP, adenosine triphosphate; DCM, dichloromethane; DFG, aspartate-phenylalanine-glycine; DIPEA, diisopropylethylamine; DMEM, Dulbecco's Modified Eagle Medium; DMF, dimethylformamide; DMSO, dimethyl sulfoxide; *E. coli*, *Escherichia coli*; ELISA, enzyme-linked immunosorbent assay; Eph, erythropoietin-producing human hepatocellular carcinoma receptor; FCS, fetal calf serum; FRET, fluorescence-resonance energy transfer; Lck, lymphocyte-specific kinase; MD, molecular dynamics; $P_{app}$, apparent permeability; PBS, phosphate-buffered saline; PEG, polyethylene glycol; PCC, pyridinium chlorochromate; SAR, structure−activity relationship; RIPK2, receptor interacting serine-threonine protein kinase 2; THF, tetrahydrofuran

## ■ REFERENCES


(1) Pasquale, E. B. Eph receptor signalling casts a wide net on cell behaviour. *Nat. Rev. Mol. Cell. Biol.* **2005**, *6*, 462−475.

(2) Adams, R. H. Vascular patterning by Eph receptor tyrosine kinases and ephrins. *Semin. Cell. Dev. Biol.* **2002**, *13*, 55−60.

(3) Martiny-Baron, G.; Holzer, P.; Billy, E.; Schnell, C.; Brueggen, J.; Ferretti, M.; Schmiedeberg, N.; Wood, J. M.; Furet, P.; Imbach, P. The small molecule specific EphB4 kinase inhibitor NVP-BHG712 inhibits VEGF driven angiogenesis. *Angiogenesis* **2010**, *13*, 259−267.

(4) Bardelle, C.; Cross, D.; Davenport, S.; Kettle, J. G.; Ko, E. J.; Leach, A. G.; Mortlock, A.; Read, J.; Roberts, N. J.; Robins, P.; Williams, E. J. Inhibitors of the tyrosine kinase EphB4. Part 1: Structure-based design and optimization of a series of 2,4-bis-anilinopyrimidines. *Bioorg. Med. Chem. Lett.* **2008**, *18*, 2776−2780.

(5) Miyazaki, Y.; Nakano, M.; Sato, H.; Truesdale, A. T.; Stuart, J. D.; Nartey, E. N.; Hightower, K. E.; Kane-Carson, L. Design and effective synthesis of novel templates, 3,7-diphenyl-4-amino-thieno and furo-[3,2-c]pyridines as protein kinase inhibitors and in vitro evaluation targeting angiogenetic kinases. *Bioorg. Med. Chem. Lett.* **2007**, *17*, 250−254.

(6) Lafleur, K.; Huang, D.; Zhou, T.; Caflisch, A.; Nevado, C. Structure-based optimization of potent and selective inhibitors of the tyrosine kinase erythropoietin producing human hepatocellular carcinoma receptor B4 (EphB4). *J. Med. Chem.* **2009**, *52*, 6433−6446.

(7) Zuccotto, F.; Ardini, E.; Casale, E.; Angiolini, M. Through the "gatekeeper door": exploiting the active kinase conformation. *J. Med. Chem.* **2010**, *53*, 2681−2694.

(8) Mitchell, S. A.; Danca, M. D.; Blomgren, P. A.; Darrow, J. W.; Currie, K. S.; Kropf, J. E.; Lee, S. H.; Gallion, S. L.; Xiong, J. M.; Pippin, D. A.; DeSimone, R. W.; Brittelli, D. R.; Eustice, D. C.; Bourret, A.; Hill-Drzewi, M.; Maciejewski, P. M.; Elkin, L. L. Imidazo[1,2-a]pyrazine diaryl ureas: inhibitors of the receptor tyrosine kinase EphB4. *Bioorg. Med. Chem. Lett.* **2009**, *19*, 6991−6995.

(9) Noberini, R.; Lamberto, I.; Pasquale, E. B. Targeting Eph receptors with peptides and small molecules: progress and challenges. *Semin. Cell. Dev. Biol.* **2012**, *23*, 51−57.

(10) Kolb, P.; Kipouros, C. B.; Huang, D.; Caflisch, A. Structure-based tailoring of compound libraries for high-throughput screening: discovery of novel EphB4 kinase inhibitors. *Proteins* **2008**, *73*, 11−18.

(11) Bamborough, P.; Angell, R. M.; Bhamra, I.; Brown, D.; Bull, J.; Christopher, J. A.; Cooper, A. W.; Fazal, L. H.; Giordano, I.; Hind, L.; Patel, V. K.; Ranshaw, L. E.; Sims, M. J.; Skone, P. A.; Smith, K. J.; Vickerstaff, E.; Washington, M. N-4-Pyrimidinyl-1H-indazol-4-amine inhibitors of Lck: indazoles as phenol isosteres with improved pharmacokinetics. *Bioorg. Med. Chem. Lett.* **2007**, *17*, 4363−4368.

(12) Jeong, E. J.; Liu, X.; Jia, X.; Chen, J.; Hu, M. Coupling of conjugating enzymes and efflux transporters: impact on bioavailability and drug interactions. *Curr. Drug Metab.* **2005**, *6*, 455−468.

(13) Manley, P. W.; Drueckes, P.; Fendrich, G.; Furet, P.; Liebetanz, J.; Martiny-Baron, G.; Mestan, J.; Trappe, J.; Wartmann, M.; Fabbro, D. Extended kinase profile and properties of the protein kinase inhibitor nilotinib. *Biochim. Biophys.* **2010**, *1804*, 445−453.

(14) Auffinger, P.; Hays, F. A.; Westhof, E.; Ho, P. S. Halogen bonds in biological molecules. *Proc. Natl. Acad. Sci. U.S.A.* **2004**, *101*, 16789−16794.

(15) Huber, K.; Brault, L.; Fedorov, O.; Gasser, C.; Filippakopoulos, P.; Bullock, A. N.; Fabbro, D.; Trappe, J.; Schwaller, J.; Knapp, S.; Bracher, F. 7,8-dichloro-1-oxo-$\beta$-carbolines as a versatile scaffold for the development of potent and selective kinase inhibitors with unusual binding modes. *J. Med. Chem.* **2012**, *55*, 403−413.

(16) Ishikawa, M.; Hashimoto, Y. Improvement in aqueous solubility in small molecule drug discovery programs by disruption of molecular planarity and symmetry. *J. Med. Chem.* **2011**, *54*, 1539−1554.

(17) Maier, J. A.; Brugel, T. A.; Sabat, M.; Golebiowski, A.; Laufersweiler, M. J.; VanRens, J. C.; Hopkins, C. R.; De, B.; Hsieh, L. C.; Brown, K. K.; Easwaran, V.; Janusz, M. J. Development of N-4,6-pyrimidine-N-alkyl-N′-phenyl ureas as orally active inhibitors of lymphocyte specific tyrosine kinase. *Bioorg. Med. Chem. Lett.* **2006**, *16*, 3646−3650.

(18) Sabat, M.; VanRens, J. C.; Laufersweiler, M. J.; Brugel, T. A.; Maier, J.; Golebiowski, A.; De, B.; Easwaran, V.; Hsieh, L. C.; Walter, R. L.; Mekel, M. J.; Evdokimov, A.; Janusz, M. J. The development of 2-benzimidazole substituted pyrimidine based inhibitors of lymphocyte specific kinase (Lck). *Bioorg. Med. Chem. Lett.* **2006**, *16*, 5973−5977.

(19) Zagorska, A.; Jurczyk, S.; Pawlowski, M.; Dybala, M.; Nowak, G.; Tatarczynska, E.; Nikiforuk, A.; Chojnacka-Wojcik, E. Synthesis and preliminary pharmacological evaluation of imidazo[2,1-f]purine-2,4-dione derivatives. *Eur. J. Med. Chem.* **2009**, *44*, 4288−4296.

(20) Baraldi, P. G.; Preti, D.; Tabrizi, M. A.; Fruttarolo, F.; Romagnoli, R.; Zaid, N. A.; Moorman, A. R.; Merighi, S.; Varani, K.; Borea, P. A. New pyrrolo[2,1-f]purine-2,4-dione and imidazo[2,1-f]purine-2,4-dione derivatives as potent and selective human A3 adenosine receptor antagonists. *J. Med. Chem.* **2005**, *48*, 4697−4701.
(21) Baraldi, P. G.; Preti, D.; Tabrizi, M. A.; Romagnoli, R.; Saponaro, G.; Baraldi, S.; Botta, M.; Bernardini, C.; Tafi, A.; Tuccinardi, T.; Martinelli, A.; Varani, K.; Borea, P. A. Structure-activity relationship studies of a new series of imidazo[2,1-f]purinones as potent and selective A(3) adenosine receptor antagonists. *Bioorg. Med. Chem.* **2008**, *16*, 10281−10294.
(22) Messaoudi, S.; Treguier, B.; Hamze, A.; Provot, O.; Peyrat, J. F.; De Losada, J. R.; Liu, J. M.; Bignon, J.; Wdzieczak-Bakala, J.; Thoret, S.; Dubois, J.; Brion, J. D.; Alami, M. Isocombretastatins A versus combretastatins A: The forgotten isoCA-4 isomer as a highly promising cytotoxic and antitubulin agent. *J. Med. Chem.* **2009**, *52*, 4538−4542.
(23) Alcalde, E.; Mesquida, N.; Frigola, J.; Lopez-Perez, S.; Merce, R. Indene-based scaffolds. Design and synthesis of novel serotonin 5-HT6 receptor ligands. *Org. Biomol. Chem.* **2008**, *6*, 3795−3810.
(24) Takami, A.; Iwakubo, M.; Okada, Y.; Kawata, T.; Odai, H.; Takahashi, N.; Shindo, K.; Kimura, K.; Tagami, Y.; Miyake, M.; Fukushima, K.; Inagaki, M.; Amano, M.; Kaibuchi, K.; Iijima, H. Design and synthesis of Rho kinase inhibitors (I). *Bioorg. Med. Chem.* **2004**, *12*, 2115−2137.
(25) Bakke, B. A.; McIntosh, M. C.; Turnbull, K. D. Improved alkylation and product stability in phosphotriester formation through quinone methide reactions with dialkyl phosphates. *J. Org. Chem.* **2005**, *70*, 4338−4345.
(26) Kumar, S. R.; Singh, J.; Xia, G.; Krasnoperov, V.; Hassanieh, L.; Ley, E. J.; Scehnet, J.; Kumar, N. G.; Hawes, D.; Press, M. F.; Weaver, F. A.; Gill, P. S. Receptor tyrosine kinase EphB4 is a survival factor in breast cancer. *Am. J. Pathol.* **2006**, *169*, 279−293.
(27) Stephenson, S. A.; Slomka, S.; Douglas, E. L.; Hewett, P. J.; Hardingham, J. E. Receptor protein tyrosine kinase EphB4 is up-regulated in colon cancer. *BMC Mol. Biol.* **2001**, *2*, 15.
(28) Castellano, G.; Reid, J. F.; Alberti, P.; Carcangiu, M. L.; Tomassetti, A.; Canevari, S. New potential ligand-receptor signaling loops in ovarian cancer identified in multiple gene expression studies. *Cancer Res.* **2006**, *66*, 10709−10719.
(29) Choi, Y.; Syeda, F.; Walker, J. R.; Finerty, P. J., Jr.; Cuerrier, D.; Wojciechowski, A.; Liu, Q.; Dhe-Paganon, S.; Gray, N. S. Discovery and structural analysis of Eph receptor tyrosine kinase inhibitors. *Bioorg. Med. Chem. Lett.* **2009**, *19*, 4467−4470.
(30) Huang, D.; Zhou, T.; Lafleur, K.; Nevado, C.; Caflisch, A. Kinases selectivity potential for inhibitors targeting the ATP binding site: a network analysis. *Bioinformatics* **2010**, *26*, 198−204.
(31) Kabsch, W. Automatic processing of rotation diffraction data from crystals of initially unknown symmetry and cell constants. *J. Appl. Crystallogr.* **1993**, *26*, 795−800.
(32) The CCP4 suite: programs for protein crystallography. *Acta Crystallogr., Sect. D: Biol. Crystallogr.* **1994**, *50*, 760-763.
(33) McCoy, A. J.; Grosse-Kunstleve, R. W.; Adams, P. D.; Winn, M. D.; Storoni, L. C.; Read, R. J. Phaser crystallographic software. *J. Appl. Crystallogr.* **2007**, *40*, 658−674.
(34) Adams, P. D.; Grosse-Kunstleve, R. W.; Hung, L. W.; Ioerger, T. R.; McCoy, A. J.; Moriarty, N. W.; Read, R. J.; Sacchettini, J. C.; Sauter, N. K.; Terwilliger, T. C. PHENIX: building new software for automated crystallographic structure determination. *Acta Crystallogr., Sect. D: Biol. Crystallogr.* **2002**, *58*, 1948−1954.